energies

MDPI

Article

A Multidisciplinary Approach to Evaluate the Environmental Impacts of Hydrocarbon Production in Khuzestan Province, Iran

Herimitsinjo Rajaoalison, Dariusz Knez * and Mohammad Ahmad Mahmoudi Zamani

Department of Drilling and Geoengineering, Faculty of Drilling, Oil and Gas, AGH University of Science and Technology, Mickiewicza 30, 30-059 Krakow, Poland
* Correspondence: knez@agh.edu.pl; Tel./Fax: +48-12-617-37-84

Abstract: From the late 1900s onward, hydrocarbon exploitation has led to severe environmental footprints in the Khuzestan province, Iran. However, no comprehensive study has been conducted to evaluate such issues. In this research, an inclusive analysis was performed to investigate these environmental impacts. To do this, first, two datasets related to a 15-year period (2006–2021) were collated: the satellite data from the Sentinel-1 mission and the seismic data recorded by the National Iranian Geophysics Institute as well as the catalog of the global Centroid Moment Tensor project (CMT). These datasets were processed using generic mapping tools (GMT), differential synthetic aperture radar (D-InSAR) techniques, and multiple processing algorithms using a specific toolbox for oil spill application in the sentinel application platform (SNAP) programming, respectively. The results revealed three critical footprints, including regional earthquakes, land subsidence, and oil spill issues in the area. The most frequent earthquakes originated from depths less than 15 km, indicating the disturbance of the crustal tectonics by the regional hydrocarbons. Furthermore, an annual rate of land subsidence equal to 10–15 cm was observed in the coastal areas of the Khuzestan province. Moreover, two regions located in the north and west of the Persian Gulf were detected as the permanently oil-spilled areas. The applied methodology and results are quite applicable to restrict the harmful consequences of hydrocarbon production in the study area. This research will benefit not only government officials and policymakers, but also those looking to understand the environmental challenges related to oil and gas production, especially in terms of sustainable goals for the management of natural resources.

Keywords: sustainable management; oil/gas exploitation; environmental footprints; land subsidence; oil spill; seismic activities; natural resources; remote sensing; Sentinel-1 mission

Citation: Rajaoalison, H.; Knez, D.; Zamani, M.A.M. A Multidisciplinary Approach to Evaluate the Environmental Impacts of Hydrocarbon Production in Khuzestan Province, Iran. *Energies* **2022**, *15*, 8656. https://doi.org/10.3390/en15228656

Academic Editor: Dameng Liu

Received: 21 September 2022
Accepted: 16 November 2022
Published: 18 November 2022

1. Introduction

Iranian oil and gas reserves have been proven to be one of the largest reservoirs in the world. They represent approximately 10% of the total world's oil reserves, that is, nearly 137 billion barrels, and 15% of the total world's gas reserves, that is, nearly 41 trillion cubic meters. It produced a daily average of 5 million barrels during the last 60 years [1]. The exploration of these natural resources has had a considerable impact on the domestic economy, as well as on the oil and gas markets worldwide. However, the hydrocarbon production from underground reservoirs has caused some environmental concerns, especially in the Khuzestan province, which is the center of oil/gas production in Iran. Such issues include frequent seismic activities, land subsidence, and oil spills over the adjacent Persian Gulf [2–4].

In general, earthquakes occur when the energy accumulated along a fault is released. A typical fault separates two compartments or blocks of rock that slide and move along the fault surface plan. During the oil/gas drilling and production phases, the initial stress state in the ground alters, leading to potential fault activation events. Consequently, the

sudden movement of the faults radiates the compressional and shear waves traveling through the upper rocks and reaching the ground surface [5–7]. On the ground surface, the waves are recorded by the previously installed seismometer in the form of time signals or seismograms. These seismograms are then used to detect the characteristics of the earthquake, such as location, size, source type, and dynamics [8,9].

In addition, the settlement of the ground surface, known as land subsidence, has been observed all over the world due to natural and induced causes. Natural subsidence occurs because of natural activities on the Earth related to tectonic activities, such as subduction, while induced land subsidence occurs due to human activities such as mining and the withdrawal of hydrocarbons [10–18]. Land subsidence with rates of more than tens of centimeters per year has occurred in numerous cities, such as Tehran (Iran) with a rate of 20 cm/year, Yunlin (China) with a rate of 10 cm/year, Mexico city (Mexico) with a rate of 9 cm/year, and Bologna (Italy) with a rate of 4 cm/year [19–21]. Generally, the impacts of land subsidence can be divided into four main categories, including (1) infrastructure damage such as buildings, pipelines, and dams, (2) foundation and service damage such as roads and railways, (3) exposure to floods during rainy seasons, and (4) groundwater pollution due to chemical intrusion into the source [22–24]. Most land subsidences have been identified to be related to the extraction of underground fluids. For example, the production of shallow and fresh water in Mexico resulted in magnitudes of subsidence of 762 cm in San Joaquin and 396 cm in California, Santa Clara Valley [25,26]. In addition to that, the first subsidence related to oil production was observed in the Goose Creek field in Texas [27–29]. In addition to the previously mentioned impacts, the infrastructure damage in the oil field itself can also be attributed to subsidence, including well failure [30–32].

Likewise, a study about the direct as well as indirect effects from underground mining was undertaken, carried out in complex geological and mining conditions, changing over time and space at Bogdanka Hard Coal Mine in the eastern part of Poland, including land subsidence and induced drainage of the aquifers. They used the Knothe theory to investigate the spatial extent of land subsidence of the area, while they used the conventional groundwater flow theory to produce the finite-difference 3D model of the underground mining-induced draining of the aquifers. The outcomes of their research have shown the direct effects of the environmental impact, such as land subsidence, but the indirect effects even have more impacts due to the extent of the depression cone outside the mining area. Apart from that, a highly relevant prediction of mining-induced drainage has been established from the 3D numerical model [33]. Another good example of mining-induced subsidence is the case of the Gippsland Basin of 46,000 km^2 in Australia, where the InSAR method was used by Ng et al., which allowed them to map that the land subsidence of the area varied between −10 and 10 mm/year, which was in accordance with the results of the GPS survey. The surrounding area of the mining sites experienced a rapid deformation of −82.9 mm/year, which was induced by the dewatering of the mining activities in the mine [34].

Many cases around the globe have proved the existence of human activities related to land subsidence, such as fluid withdrawal, including groundwater and hydrocarbons, and mining activities, which have been identified all over the world by scientists using different methods including remote sensing. For example, Deng et. al. has studied the surface deformation and induced seismicity of the Permian Basin in West Texas using the InSAR time series, which is experiencing an increase in seismic activity and is probably related to the production process of oil and gas in the largest sediment basins in the west and southeast of New Mexico and one of the most productive oil and gas basins in the United States. Recent increases in seismicity in West Texas were likely related to oil and gas production according to temporal and spatial correlations [25]. Additionally, land subsidence in coastal areas, coastal plains, and river deltas in Tabasco in Mexico has been studied using the differential interferograms stacking (DIS) approach together with D-InSAR techniques, in which a subsidence of 6 cm/year has been investigated as related to urban growth in other localities, which may influence the susceptibility to flooding;

the possibility of a link between surface deformation and hydrocarbon extraction in the affected region has been suggested on the basis of the obtained results [35]. In addition, Liu et al. studied the link between hydrocarbon exploitation and land subsidence over the Yellow River delta using the multi-temporal InSAR technique. They established a pattern and magnitude of land subsidence of the oil fields area. Their studies confirmed that hydrocarbon exploitation activities induced and accelerated land subsidence in the area, as it plays the most dominant role in the Yellow River delta. A good consistency between the distribution of faults and subsidence has been identified, in which the subsidence and uplift areas expand over time over the Shikou oil field and can reach an approximate annual average of 40 mm/year and less than 35 mm/year over the Dongying oil field [36]. Moreover, Kuzmin found that the long-term development of subsidence was absent when he studied the deformation consequences at oil and gas fields and underground gas storage in Russia and Turkmenistan, while the injection of gas into the underground storage produced local subsidence [37]. For the same reason, Macini et al. explained the case of monitoring of land subsidence and seismicity and pore pressure around oil and gas production after the Emilia earthquake of 2012, which caused some casualties and damage to some buildings and industrial infrastructure in Po plain province in Italy, where a large number of oil and gas settled, in which the production process was in its final stage at the time. Therefore, policies have been drawn between involved entities and governments to monitor the ground deformation of the region in systematic ways and provide published reports every 12 months, preferably by 6 months. The involvement of fluid injection into the formation must be minimized and preserved as equal to its original state due to the fact that such a process considerably affects the pre-existing stress in the reservoir, which triggers microseismic events and, therefore, subsidence [38].

Regarding pollution issues derived from the oil/gas industry, a critical illustration is oil spill contamination [39–41]. Oil spill contamination is a real global tragedy in which oil produced on offshore platforms, refineries, or oil tankers is spread over the oceans. It can naturally occur through seepage from oil structures below the sea bed or from anthropogenic activities such as ship accidents [42–44]. The oil spill affects the ecosystem in many ways, depending on its chemical composition, the area, and the cleaning activities. It is still considered a major pollutant of the oceans among other pollutants, making it a real threat to coastal environments [45,46]. Approximately 45% of global ocean oil spills are attributed to human sources, while the mean share of transportation is only approximately 5% [43,47]. Some examples of catastrophic events of oil spills include the Amoco Cadiz in France in 1978, the Exxon Valdez in Alaska in 1989, in Kuwait during the Gulf War in 1991, in France at the Erica in 1999, Galicia, Spain in the Aegean Sea in 1992, and at the Prestige in Spain and France in 2002 [48]. Four characteristics define the persistence and behavior of oil in the sea, including relative density, distillation characteristics, viscosity, and pour point [49].

In addition to the abovementioned environmental issues, there are other types of footprints which are derived from industrial projects such as oil/gas operations, including the disposal of drilled rock cuttings that contaminate surface soil and water resources similar to global mining activities [50]. Moreover, the gas flaring and the emission of greenhouse gases into the atmosphere are other illustrations of such environmental impacts. Such gaseous pollutants can be prevented from being released into the atmosphere using modern carbon storage techniques [51].

From the late 1900s, the huge oil/gas reserves in the Khuzestan province have been exploited and depleted. Such anthropogenic activities have given rise to numerous environmental impacts on the regional ecosystem. Based on real observations, the severity and frequency of such impacts are being intensified as such issues are left unsolved by the petroleum companies and the regional authorities.

The objective of this research is to provide an inclusive scrutiny on the most threatening environmental footprints driven by oil/gas exploitation in the Khuzestan province, Iran. For this purpose, two categories of raw data were adopted: the first category was the

regional seismic data recorded by the National Iranian Geophysics Institute located in Tehran. These data were analyzed to correlate the magnitude and source of regional earthquakes with the oil/gas exploitation operations conducted in the Khuzestan province. In addition to that, the catalog of the global Centroid Moment Tensor project (CMT) was used to understand the main driven fault types in the region. The second category was the satellite data taken from the Sentinel-1 mission, which were analyzed to quantify the land subsidence and oil spill events in the study area. According to the conducted research, the oil/gas exploitation has activated the initial tectonics regime of the regional ground, thereby leading to the occurrence of frequent shallow earthquakes. Moreover, such operations have brought about remarkable land subsidence (10–15 cm per year) and permanently oil-spilled areas (in the northern and western parts of the Persian Gulf).

Although the extent of the oil spill areas was found to be significant in the vicinity of Khuzestan province, tracking and determining the main sources of oil spill contaminants has remained unsolved. Such contaminations may originate from offshore oil wellbores, subsea oil pipelines, or oil ships. Hence, for future works, it is necessary to address this issue.

The structure of this article is as follows: Firstly, in Section 2, the geographical and geological characteristics of the study area are elaborated. Moreover, the history and dispersion of the primary oil/gas fields in the region are presented. Then, in Section 3, the applied methodology is described. Afterwards, in Section 4, the key achieved results are presented and discussed. Ultimately, the article ends with a concise description related to the main findings, propositions, and conclusions.

2. Geology and Tectonics of Iranian Oil and Gas Fields

The surface of Iran includes approximately 2300 km through the NW to SE direction. The entire topography map of Iran, together with the investigated area, is presented in (Figure 1A). In this figure, the study area including Khuzestan province and the northern part of the Persian Gulf is shown by a red box. The reconstruction of the Paleo-Tethys and Neo-Tethys oceans formed the three main structural units of the Iranian plateau, which are (1) the Zagros-Makran orogenic system, (2) the central Iranian microplate, and (3) the NE Turan part of the Iranian plateau. Subduction and subsequent collision of Neo-Thetys formed the Zagros-Makran orogenic system, while amalgamation of Cimmerian blocks in Eurasia formed the Central Iranian microplates [52,53]. The western and southern parts of the Iranian plateau constitute the NW–SE to the E–W direction trending the Zagros-Makran orogenic belt. Consistent with constraints, the northern part constitutes the Talesh-Alborz-Kopeh-Dagh belt trending the southern Caspian basin as well as the edge of Eurasia [54,55].

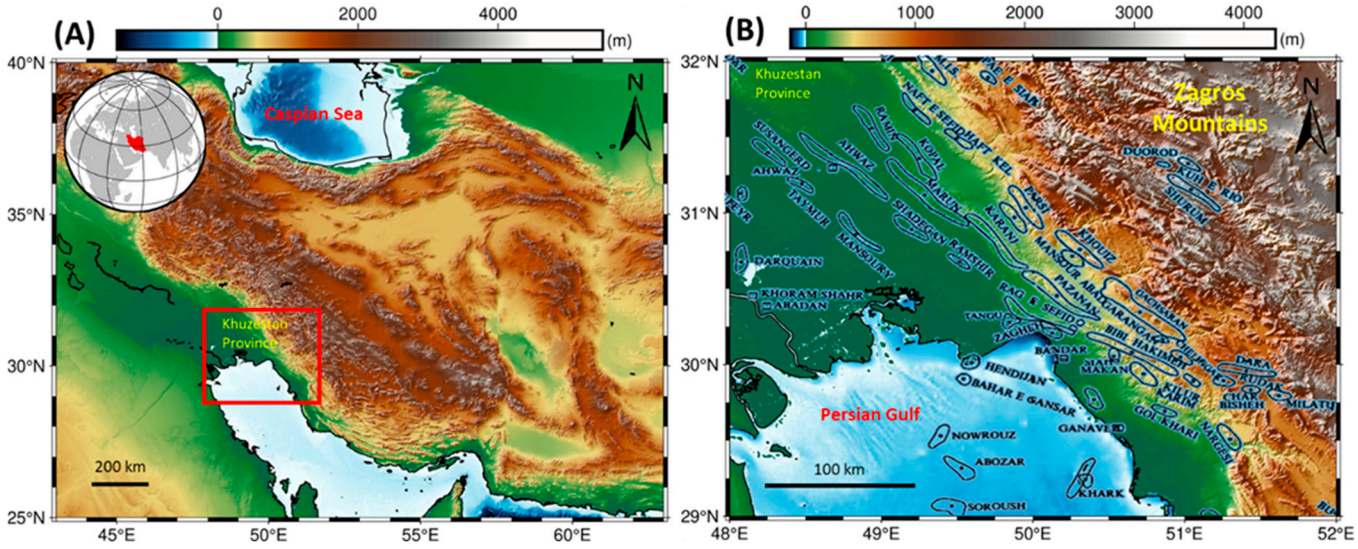

Figure 1. Topography of (**A**) Iran and (**B**) the location of oil/gas fields in the study area.

Figure 1B illustrates a close up of the study area. As it is shown, the study area encompasses the Khuzestan province as well as the northern part of the Persian Gulf. The locations of the offshore and onshore oil/gas fields have also been shown in the figure. In the north of the Khuzestan province, the Zagros Mountains are located. From those mountains, several large rivers, e.g., Karoon, Dez, Karkheh, etc., originate and flow through the Khuzestan province towards the Persian Gulf. Regarding the topography of the province, the northern parts are highlands with an average altitude of 2500 m. By contrast, southern terrains are in the form of relatively flat fertile lands producing a wide range of agricultural crops, such as wheat, barley, corn, dates, etc., with an average altitude equal to 100 m.

In 1908, the first Iranian oil wellbore was drilled in the Masjed Soleiman city, situated in the north of the Khuzestan province. Since then, the province has been the main center of hydrocarbon production in Iran. There are many offshore and onshore oil/gas fields in the study area (Figure 1B). While the onshore fields are spread throughout the entire region, the offshore fields are located in the Persian Gulf, where more than 51% of recoverable liquid hydrocarbons are located in Cretaceous reservoir rocks and 50% of gaseous hydrocarbons are found in Premo-Triassic formations. Furthermore, approximately 80% of the oil reserves lie in carbonate formations, while only 20% are trapped in sandstone rocks. The underlying sediments beneath the Persian Gulf have a thickness of up to 10,000 m, and the section is a relatively continuous and conformable sequence from the Infra-Cambrian to the Pliocene [1,56].

The two most productive reservoirs in Iran include Asmari and Bangestan, which contain 43% and 25% of the entire domestic Initial Oil-In-Place (IOIP), respectively. The geological formation of these two large reservoirs can be found in most Iranian oil fields [56,57]. The first and most prolific reservoir in the study area is the Asmari formation. This formation in the Khuzestan province includes wackestone and packstone with different thicknesses of 320 to 488 m with a relative length of 10 to 280 m comprising effective reservoirs. The age of formation dates to the Oligocene-Miocene period. The cap rocks of the Asemari formation are the evaporites related to the salty Gachsaran formation. Moreover, the primary porosity of the reservoir is usually less than 5%, while the secondary porosity reaches 25% as a result of fracturing. Furthermore, the average permeability of the formation was measured around 10 mD and increased to 100 mD in highly fractured segments [57].

The second most productive formation in Iran is the Bangestan reservoir. It consists of two formations, including the older Sarvak and the Ilam formation. The Bangestan reservoir is made up of massive and shallow marine limestone. The gross and net thickness ranges of these two reservoirs have been calculated at around 220 to 980 m and 70 to 630 m, respectively. The common porosity domain is approximately 4 to 15%. The lithology of the older Sarvak formation consists of limestone and chert rocks. Moreover, the porosity is in the range of 7 to 14%. The Ilam formation is made up of argillaceous limestone and shale with a porosity range of 9 to 20% [58].

3. Materials and Methods

This section presents the methods used to assess the environmental impacts related to the oil and gas production in Iran. Such methods included monitoring of local earthquakes and major earthquakes for several decades, monitoring of land subsidence near the production area, and monitoring of oil spills in the Persian Gulf. At first, the earthquake monitoring is presented with the history of the Iranian seismic local network. Then, the use of satellite images to investigate the change observed on the ground surface as the result of oil and gas production is elaborated. Finally, the results of the oil spill events in the Persian Gulf are presented.

3.1. Earthquake Monitoring and Focal Mechanisms

Bulleted local earthquakes in Iran have been recorded in Tehran since 1958 by the first seismic station constructed by the Institute of Geophysics, that is, an institute affiliated

with the University of Tehran. The number of analog seismic stations increased to five in the 1960s and was installed in five cities in Iran, including Tehran, Tabriz, Mashhad, Shiraz, and Kermanshah [59,60]. The number of seismometers has increased in the 20 local seismic networks in the most earthquake-prone areas of the region and form the current Iranian seismological network composed of 112 digital seismic stations and 1 borehole station (Figure 2) [61]. The magnitudes of the earthquakes were calculated and corrected using the magnitude of the Nuttli scale (Equations (1) and (2)) [59,62,63].

$$M_N = \log(\nu/4\pi) + 1.66\log(d) - 0.1 \; d \leq 106 \text{ (km)} \quad (1)$$

$$M_N = \log(\nu/4\pi) + 2.50\log(d) - 1.8 \; 106 \leq d \leq 600 \text{ (km)} \quad (2)$$

where M_N—the magnitude of Nuttli, ν—the maximum amplitude (in ηm/s), and d—the epicentral distance (in km).

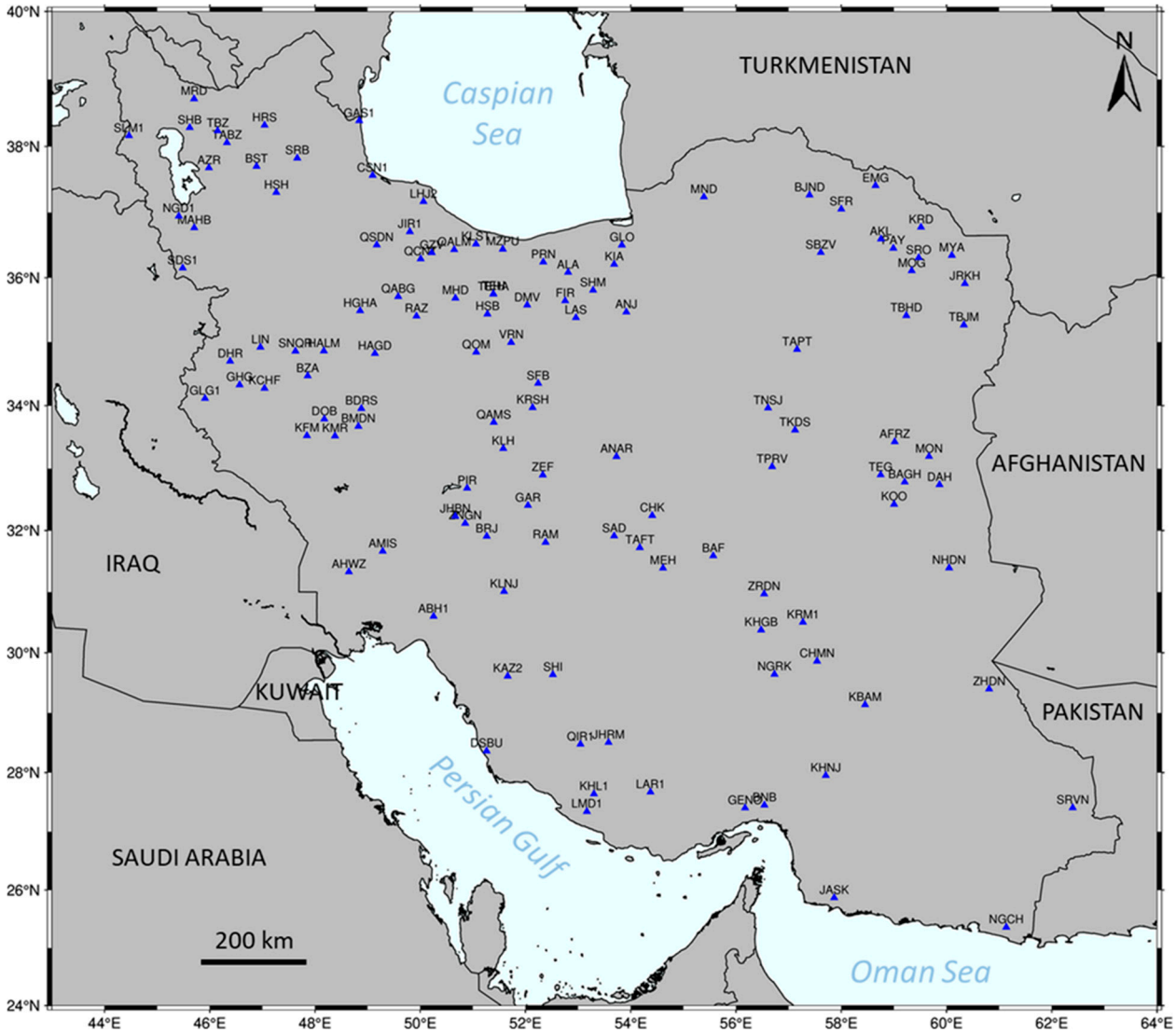

Figure 2. Coverage of Iran's active seismic local network.

Major earthquakes are often shown by focal mechanisms, which commonly have three characteristics, including strike, dip, and rake. The strike Φ, the clockwise angle from the north, is between and/or equal to 0° and 360°. The dip δ, the angle from the horizontal, is between and/or equal to 0° and 90°. The rake λ, the angle between the strike line (surface faulting) and the slip vector, is between and/or equal to −180° and 180° [64].

The movement between the two blocks, the foot wall and the hanging wall, is defined by the rake angle.

In this study, the recorded earthquakes from 2006 to 2021 by the Iranian Seismological Network within the investigated area were used to map seismic activities with magnitudes less than 5; while the catalog of the global Centroid Moment Tensor Project (CMT) (website www.globalcmt.org, accessed on 25 March 2021) developed by Adam M. Dziewonski and the Iranian Regional Centroid Moment Tensor catalog were used to understand the source characteristics and dynamics of major earthquakes with magnitudes greater than 5 between 1976 and 2021 of the area concerned [65,66]. The linear relationship between the elastic vibrations of an earthquake and the six independent elements of the zeroth-order moment tensor defines the CMT method of the global and regional catalogs in this study [67]. Generic Mapping Tools (GMT) version 6.2 was used to create the map, which is an open toolbox for earth, ocean, and planetary Science, especially for mapping [68].

3.2. Land Subsidence Monitoring

There are two ways to measure land subsidence; the first is through conventional methods, such as ground leveling and the global positioning system (GPS), which are based on measurement points. The second category is the remote sensing method using satellite images, for instance, synthetic aperture radar (SAR) images, which benefit from large coverage and precise measurements [21,69]. The differential SAR interferometry (DInSAR) technique is part of the InSAR method that was developed in the late 1990s for measuring earth deformation and presents many advantages compared to the traditional one, including large coverage, high accuracy, and fast tracking at a low cost [29,70,71]. The efficiency and accuracy of the DInSAR method have been examined in many cases around the world [27,71,72]. Multiple processing steps were carried out to quantify the subsidence related to oil and gas production in this work (Figure 3A) [73].

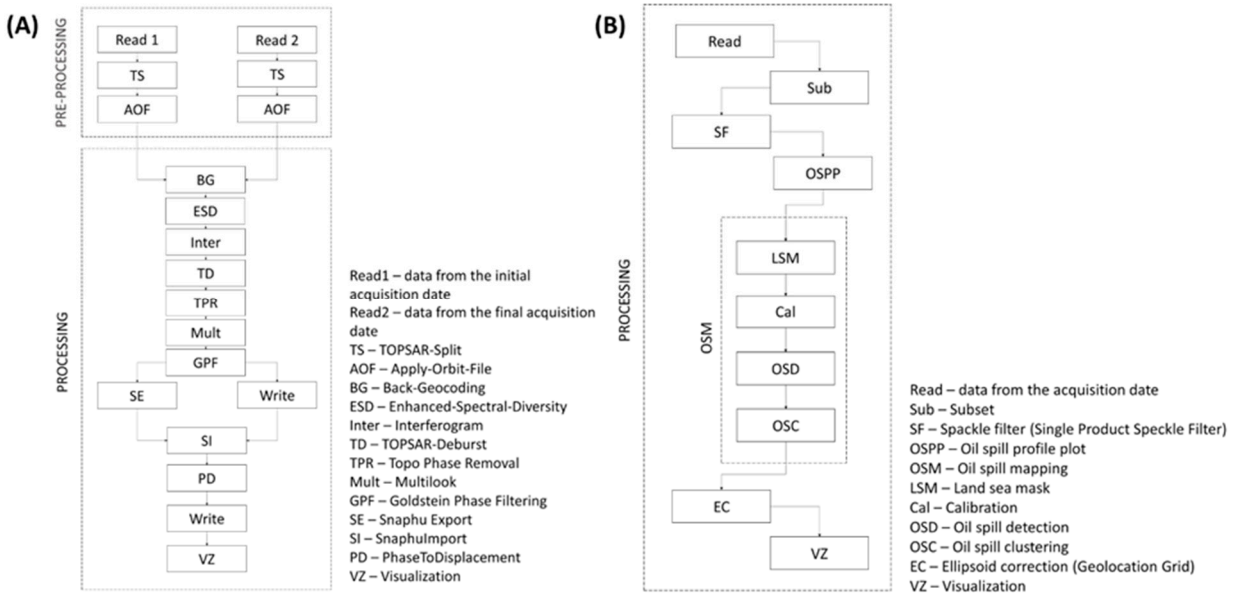

Figure 3. Data processing algorithms for (**A**) land subsidence detection and (**B**) oil spill detection in the SNAP tool.

Five types of phases make up the InSAR phase, including the topographic phase, the deformation phase, the atmospheric effect phase, the flat earth phase, and the noise phase. The following expression (Equation (3)) presents the relationship between them [29,72]:

$$\varphi = \varphi_{topo} + \varphi_{disp} + \varphi_{atm} + \varphi_{flat} + \varphi_{noise} \quad (3)$$

where φ_{topo} is the phase due to topography, φ_{disp} is the phase due to the Earth surface displacement, φ_{atm} is the phase due to atmospheric effect, φ_{flat} is the phase due to flat earth, and φ_{noise} is the noise phase.

The interferogram phase subtracted by InSAR or a digital elevation model (DEM) can be used to estimate the phase from topography [74]. The differential interferogram can be extracted using the two-pass technique, the three-pass technique, or the four-pass technique, which, utilize two, three, or four single look complex (SLC) SAR images, respectively, plus a DEM with high precision [74–76]. The coherence between the images is high when the acquisition time interval is short. In our case, the time interval is one year, which is suitable for such an application. The rest of the phase is due to the deformation of the Earth's surface within the time interval. The topography of the monitored area must be removed to obtain the displacements that occur. The deformation along the sight line is defined by Equation (4):

$$\Delta R = (\lambda / 4\pi)^* \Delta \Phi \quad (4)$$

where ΔR is the Earth's surface displacement in the satellite line of sight (LOS), λ is the wavelength, and $\Delta \Phi$ represents the differential interferometric phase.

In this study, the two-pass technique was used to construct the differential interferogram using SAR images acquired on 3 February 2020 and 28 January 2021 (website, https://scihub.copernicus.eu/, accessed on 10 February 2020). The data used belong to Sentinel-1A products from the Sentinel mission of the European Space Agency (ESA), free for use, and the algorithm for data processing has been carried out on the Sentinel Application Platform (SNAP), which is an open source software for SAR data processing [73]. Sentinel-1 was the first space mission of the ESA for the Copernicus initiative, in which one of the goals was to map surface displacement. In this case, it was used to map the subsidence related to oil and gas exploration.

3.3. Oil Spill Monitoring

Remote sensing is quite efficient in the detection and assessment of oil spills in the oceans. This effectiveness has been weighted using both active and passive techniques. The passive technique uses visible and thermal infrared of the electromagnetic spectrum to detect, map, and discriminate spilled oil [77,78]. However, it encounters many sources of noise because it is affected by cloud cover, sun glint, low contrast, etc. [79,80]. On the contrary, the active technique using synthetic aperture radar (SAR) overcomes these sources of noise, as it can operate in all weather conditions, day and night, and is even capable of covering a large area [81–83].

Sentinel-1A products, characterized by the wide swarth (IW) with a resolution of 5 m $\times$ 20 m and ground range detected (GRD) data, were used in the current study [83]. These datasets were acquired based on availability (website, https://scihub.copernicus.eu/ accessed on 10 February 2020) from February 2020 to January 2021, one per month for a year-long period. Multiple processing steps were carried out using a specific toolbox for oil spill application in SNAP programming (Figure 3B). The oil spill has a dark color in the SAR image with high contrast due to the absence or weak wave return to the SAR satellites through the spilled area [42]. Radar backscattering is reduced through small capillary waves of mineral oil that humidify the ocean surface, making the area smoother due to the reduction in surface tension [81,84]. Many cases of oil spills have been tested using the single and dual polarized SAR images, and showed efficiency, in which the vertical transmits vertical receives (VV) polarization is suggested as ideal compared to the horizontal transmits horizontal receives (HH) polarization, due to its better discrimination of the look-alike phenomenon from extreme conditions, such as thunderstorms, wind shadows, etc. [45,80,85,86].

4. Results and Discussion

4.1. Earthquakes Monitoring and Focal Mechanisms

The first result is concerns earthquake monitoring. Six maps were produced after adopting the existing seismic record catalog data from more than 15 years, from 2006 to 2021, and the global and regional Centroid Moment Tensor catalog. Figure 4A presents medium earthquakes with magnitudes in the range of 2.5 to 5 and from 2006 to 2020. Figure 4B shows the corresponding results between 2020 and 2021. Figure 4C presents microearthquakes with a magnitude less than 2.5 from 2006 to 2020, while Figure 4D presents microearthquakes between 2020 and 2021.

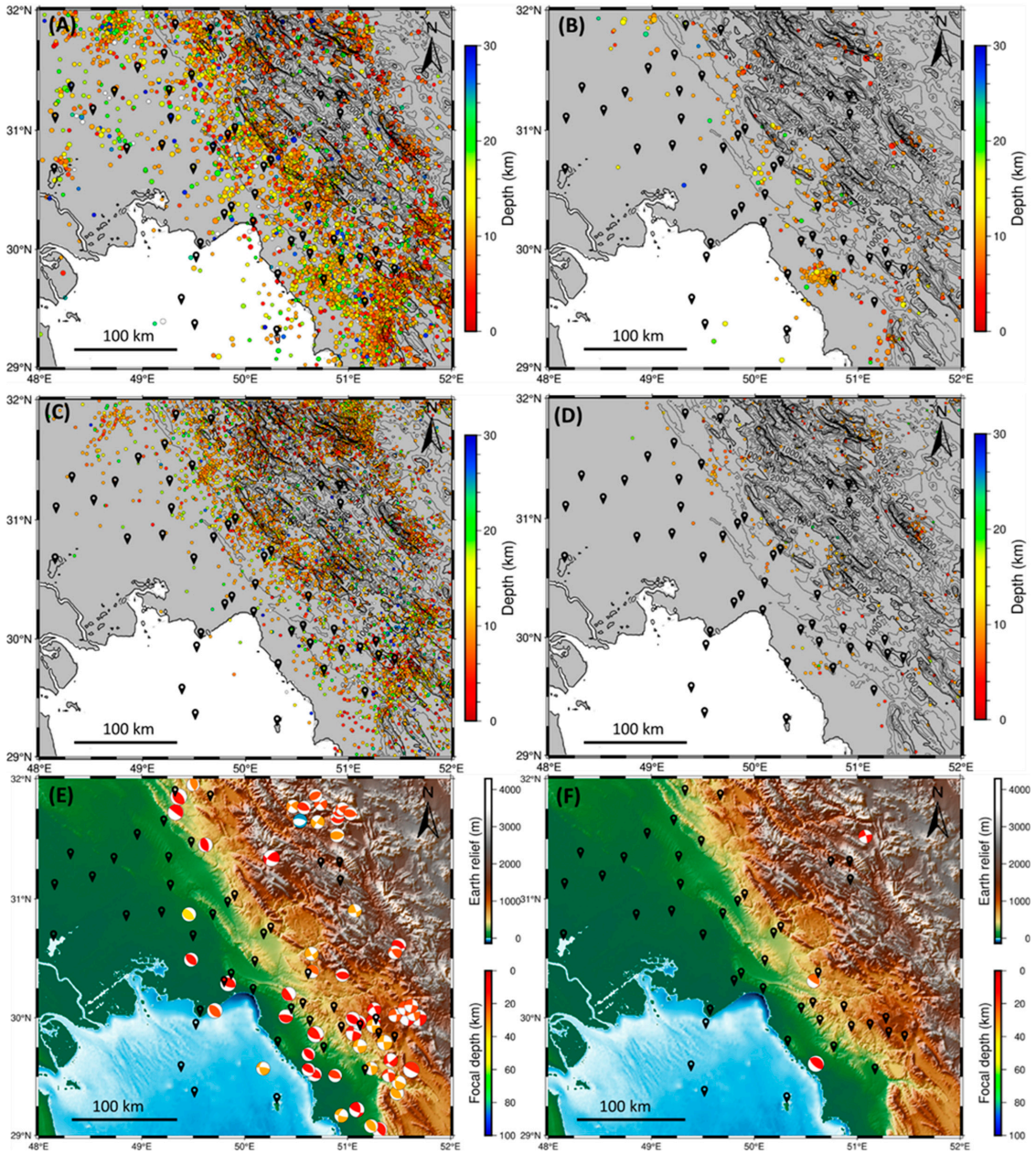

Figure 4. Seismic activities with magnitudes less than 5 and focal mechanisms of major earthquakes with magnitudes greater than 5 in the southwest part of Iran: (**A**) from 2006 to 2020 and (**B**) from 2020 to 2021 are classified as medium with magnitudes between 2.5 and 5; while (**C**) from 2006 to 2020 and (**D**) from 2020 to 2021 are classified as micro with magnitudes less than 2.5; (**E**) from 1977 to 2020 and (**F**) from 2020 to 2021. The black icons indicate the locations of the oil and gas fields.

In Figure 4, most earthquakes have a depth of around 15 km or less. Only a few of them have a depth greater than 15 km. The origin of such shallow seismic activities implies that a new change is disturbing the tectonics of the local crust. According to field surveys and the history with more than 100 years of oil extraction in the region, such seismic activities can be attributed to hydrocarbon exploitation activities in the area. These earthquakes are fairly distributed throughout the investigation area, in which most of them occurred in the eastern and northern parts, and along the NW–SE direction of the investigated area, where the oil and gas production settled. It is important to note that oil and gas exploration and production change the original stress underground, making the area susceptible and sensitive to accumulated energy release, which causes earthquakes [87]. Furthermore, this area is known to be highly tectonically active, so adding even a small change to the local stress regime can activate existing faults or natural underground cracks. The earthquakes in the southern part of the subject area showed an existing relationship between production and the earthquakes that occurred, as they had occurred very close to the production areas (Figure 4). The recorded earthquakes from 2020 to 2021, in the southeast part of the study area, confirmed their occurrence near the production area (Figure 4B,D).

Figure 4E presents the major earthquakes and their focal mechanisms between 1977 and 2020, while Figure 4F presents the major earthquakes between 2020 and 2021. The major historical earthquakes between 1977 and 2020 in the region had depths of less than 20 km, few had depths greater than 20 km, and only one event had a depth greater than 80 km. Most of the major earthquakes in Iran were shallow (Figure 4E). The tectonics of the investigated area have been run by reverse movements known as subduction and strike-slip movements, which are confirmed by the focal mechanisms of the major earthquakes of the region. In the NW–SE direction, the trend is dominated primarily by reverse faults, while the southeast part is dominated primarily by strike-slip faults. In the northeast part of the area, a combination of normal faults, strike-slip faults, and reverse faults was observed. Many of those major earthquakes occurred in oil production areas, such as in the northwest part, in the center close to the shore, and in the southern part. Therefore, oil and gas production definitely contributes to the occurrence of earthquakes, even the major ones. It is important to note that these assumptions are based on existing data.

4.2. Land Subsidence Monitoring

In addition to seismic activities, the one-year subsidence of the region's land is presented in Figure 5. The highest recorded subsidence of the affected area within one year was approximately 24 cm, and the uplift was 5 cm. A subsidence of around 5 cm was recorded in oil-gas fields in the northwest part, while 10–15 cm were recorded in the eastern and southern parts (NW–SE trend) of the investigated area. A high spot of the subsidence of around 15 cm was located near the shore in the west-center part of the investigated area, which is assumed to be from oil and gas production, as this area is typically prone to high extraction. During the past century, the main conventional reservoirs in south Iran have been exhausted and depleted by the national oil company. The extraction of such a large amount of hydrocarbon has had such an impact on the subsidence of the land. Regions that host oil fields also often experience continuous low-scale earthquakes for a few months. Cities in the Khuzestan province have experienced many types of earthquakes.

Furthermore, surface rupture after earthquakes can cause subsequent land subsidence phenomena in the form of rapid dropdown of the surface. In Iran, the observed 24 cm subsidence is located in the northwestern part of the Persian Gulf a, and it is probably associated with the major earthquakes that occur. Some studies conducted in California using benchmark elevations have proven the possibility of the relationship between tectonic activity and subsidence on the surface [10,30,88]. However, the change observed on the surface in California is not much due to the varying intensity, the severity of ground motion at a particular location of the Earth's crust (Mercelli scale), as well as the epicentral location of the earthquakes. Shaking and surface faulting are the two types of earthquakes that cause subsidence. For more than 20 years, three out of a dozen earthquakes with

magnitudes greater than 6 resulted in displacement on the surface in Kern Co, including 122 cm of vertical displacement and 61 to 91 cm of horizontal displacement from the 7.7 magnitude earthquake in 1952, 91 cm vertical and 152 cm horizontal displacement from the 6.6 magnitude earthquake in San Fernando in 1971, and only 10 cm from the 5.6 magnitude earthquake in Parkfield in 1966 [10]. In this study, since this area is tectonically active and is clearly characterized by high-magnitude reverse faults, the subsidence of the tectonic activity was greater than the subsidence derived from oil and gas production. However, these two sources are interrelated because oil and gas production changes underground stress and could trigger earthquakes. The magnitude of uplift of up to 9 cm in the northeast corner of the study area is also considered a signature of reverse faults, where the red part indicates the subsided area and the blue part represents the uplifted area.

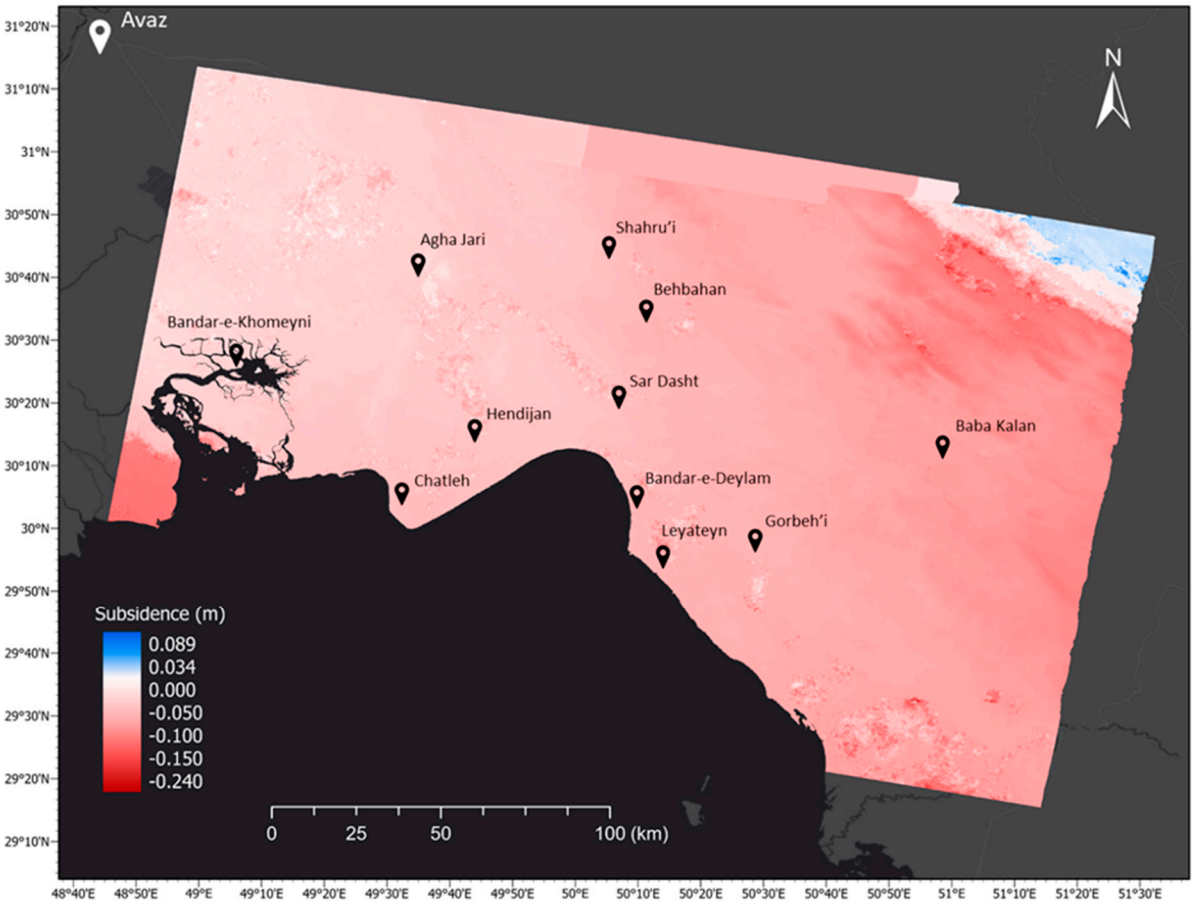

Figure 5. One—year land subsidence of the southwestern part of Iran, between February 2020 and January 2021.

4.3. Oil Spill Monitoring

In the same way, Figure 6 shows the oil spill in the ocean (Persian Gulf) for a period of one year, from February 2020 to January 2021. It shows that the Persian Gulf is always affected by oil spill contamination, but the monthly amount is different. The largest offshore oil spill over the investigated area occurred in May 2020 (Figure 6D), July 2020 (Figure 6F), October 2020 (Figure 6I), December 2020 (Figure 6K), and January 2021 (Figure 6L). The area that always has spilled oil for these 12 months is located in the northern and central western parts of the sea. The average depth of the Persian Gulf is in the range of 35–40 m and the whole area is 240 km^2. The water change period lasts 3 to 5 years, implying that it takes a long time for the seawater to be refreshed and cleaned from oil spill pollution [89,90]. Furthermore, the northern parts of the Gulf that are demonstrated in Figure 6 are subject to further contamination, as they have a deeper shallow depth, a higher degree of salinity, a

higher fluctuation of temperatures, and less water circulation. Therefore, during different seasons, changes in natural weather, together with anthropogenic origins, can affect or amplify the degree of pollution in the area. Kamranzad et al. investigated the effect of seasonal wind on the propagation of oil pollutants in the Persian Gulf [91]. It turned out that pollutants are mainly circulated from the southern parts of the gulf to the shallow-depth northern parts. In other words, they found that the transmission trajectory of the pollutants is anticlockwise and from the south to the north. The extent and density of the contamination were attributed to the seasonal wind speed. They monitored the wind speed in the different parts of the Persian Gulf. Wind speed was concluded to have the highest values in the winter and then gradually decreased during the spring, summer, and fall seasons. The maps in Figure 6 demonstrate the dispersion of the oil spill over the surface of the Gulf in different months. However, tracking the principal rationales requires a large-scale investigation of current active pollutions over the gulf surface, wind speed, continuous monitoring of the oil extraction activities, oil ships, etc.

The cross section of backscattered wave signals across the spilled oil on the gulf in January 2021 is presented in Figure 6L. It shows a clear difference between the normal amplitude of the backscattered signal over the ocean and over the oil-spilled ocean. In this case, the oil-spilled area was characterized by a low-amplitude signature of the VV polarization of the wave reflected back to the satellite (Figure 7).

The marine ecosystem is a place where animals and plants live. The adaptation of plants and animals to live in such ecosystems depends on the physical characteristics, such as temperature, water salinity, substrata type, depth, intensity of light, and wave exposure. The oil spill affects this ecosystem in a different way because it is very sensitive to hydrocarbon contamination. On the one hand, the short-term effects depend on oil toxicity, reduction in light transmission that affects photosynthesis, dissolution of oxygen, asphyxia, and, of course, a danger to marine birds. On the other hand, long-term effects encompass the change in the biological process within the ecosystem, resulting in reproduction and recruitment disorders, disappearance of food, and habitat destruction [92–95]. Animals, for example, fish, birds, marine mammals, and even humans, are victims of food resources such as plankton, algae, eggs, and larvae which have been contaminated by dispersed oil. The most appropriate and least aggressive measure to take for illumination of an oil spill depends on the chemical composition of the oil, the affected ecosystem, and the durability of the spill [89,96,97]. It includes the appropriate coordination of the personnel involved and the materials used. It is important to preserve the unaffected area as soon as possible and remove the spilled oil in large quantities, followed by specific cleaning according to the type of affected area, sedimentary or not [98–101].

4.4. Specific Environmental Challenges in the Khuzestan Prvoince in Iran

The Khuzestan province is considered to be the center of oil and gas resources in Iran. Generally, oil/gas operations are carried out throughout the whole area of the Khuzestan province and have led to a wide spectrum of environmental footprints, such as gas flaring into the atmosphere (Figure 8A), excessive road construction, substantial pipeline networks, vegetation removal, drying the marshes, regional dusts, and waste disposal. The three latter footprints have increased dramatically during the last two decades and have caused a lot of damage, especially to human life, as well as to plant and animal ecosystems. In the following sections, the environmental footprint related to those three issues is concisely presented.

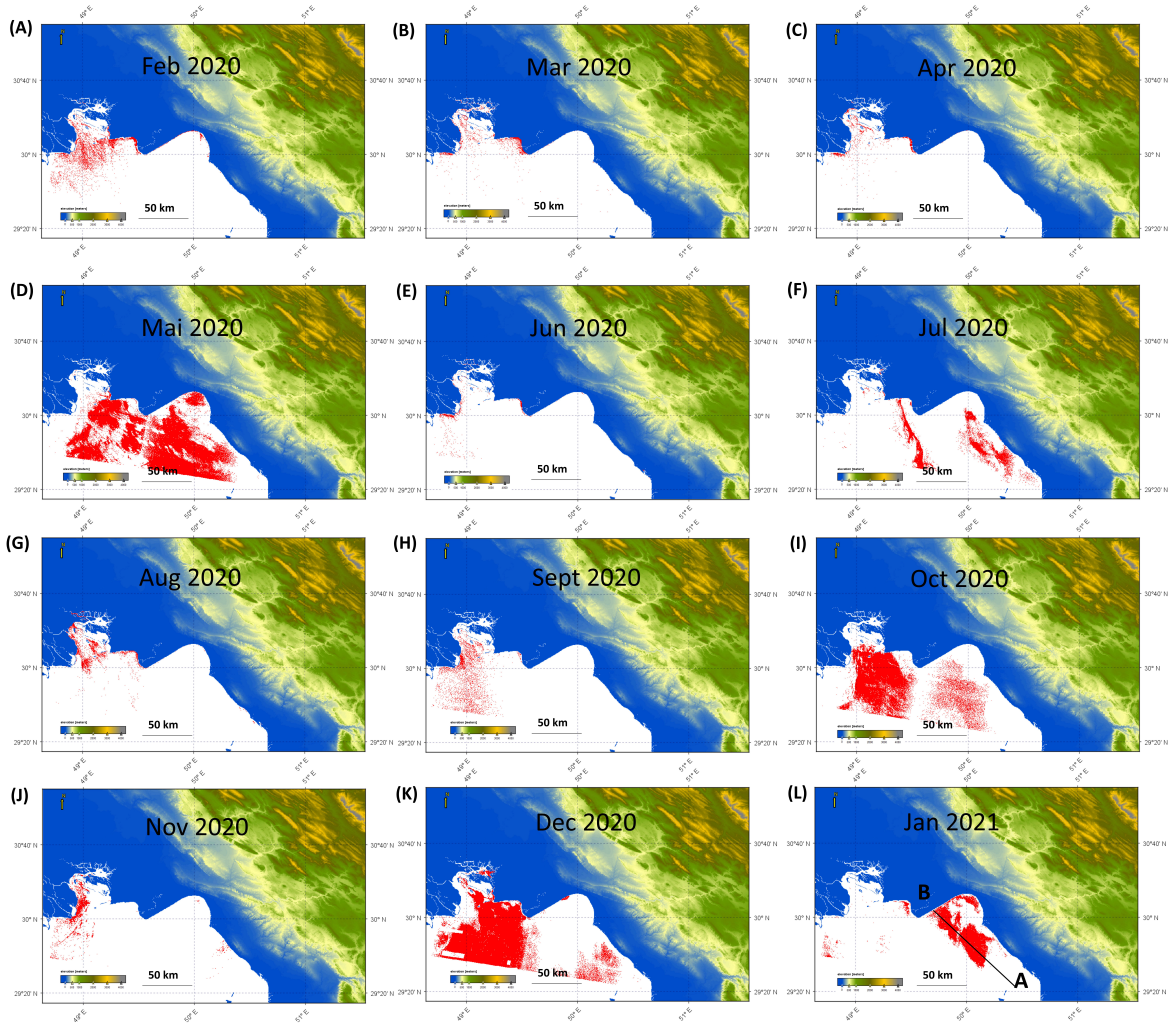

Figure 6. Offshore oil spilled over the sea (in red) near the Bahar-e-Gansar and Hendijan oil fields for 12 months. Letters (**A**–**L**) represent the months February 2020 to January 2021, respectively.

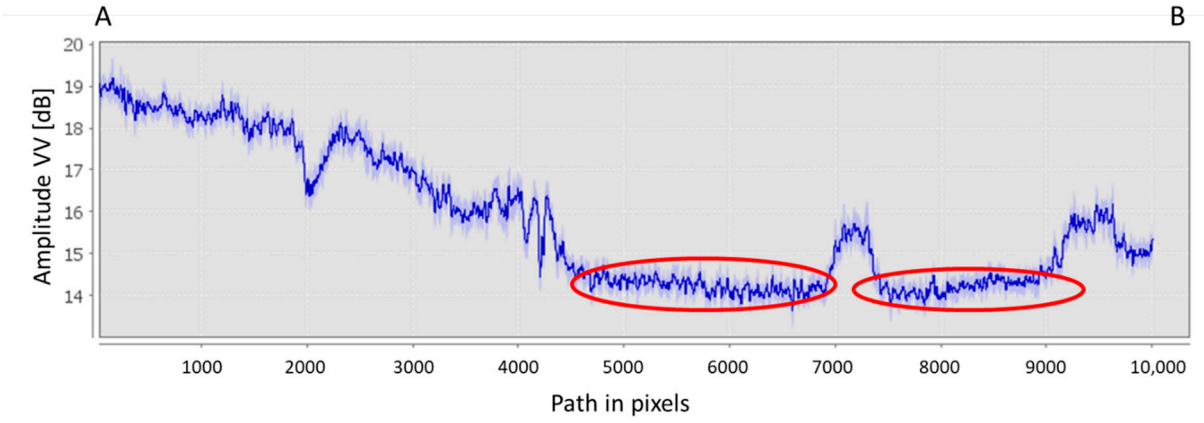

Figure 7. An example of an amplitude signature profile of vertical vertical polarization reflected waves over the oil spill across the Persian Gulf's surface through the NW–SE direction (AB cross section) in January 2021 (see Figure 6L).

Figure 8. An onshore oil drilling site in the Havizeh marsh, Khuzestan province, Iran: (**A**) contamination of the marsh water in the early stages of the drilling operation, and (**B**) water drainage and drying the entire marsh surface around the drilling site.

The discovery of oil in the marsh began in 1997, and, from 2009, oil companies began producing from the oil reservoirs located under the marsh area [56,57]. The problems were raised when the oil companies decided to divide the marsh into shorter parts by drainage water and providing dry land for the preparation of drilling sites (Figure 8) and road construction between the wellheads. This turned the marsh into a large dry area with disconnected water parts.

Figure 8 depicts an onshore oil drilling platform in the Havizeh marsh. Figure 8A shows the early stages of the drilling operations, which contaminated the water with plastic waste. On the other hand, Figure 8B illustrates the dried marsh as a consequence of water drainage carried out by the corresponding drilling company. Such actions have threatened the life of the marsh [102]. This has also led to the lowering of the ground water table in the region.

Moreover, between 2009 and 2018, a large dust propagation started in the area and the wind transferred the dust throughout the whole area of the Khuzestan province. It caused serious impacts, including lung problems for inhabitants, especially children, excessive diseases of oak trees in the Zagrous mountains, and acid rain during rainfall in the area. Recently, environmentalists have put pressure the on oil/gas companies to connect sepa-

rated water parts and restore the marsh. However, both companies in the Iran and Iraq territories show a low tendency to stop most of their activities in the marsh areas.

Khuzestan province hosts the major rivers of the country, including the Karun, Dez, Karkheh, and Jarahi rivers. All these rivers originate from the Zagros mountains (average elevation higher than 2500 m) and flow toward the Persian Gulf in the south (elevation of zero). Most of the land in the Khuzestan province is flat and without hills or mountains. These rivers have created several natural marshes in the province that are exceptional locations for many different birds and animals, as well as adjacent human colonies. The most important marsh, called the Havizeh marsh, is located in the western part of the province on the border between Iran and Iraq. This marsh has an area of 48,131 hectares. One-third of the marsh is fed by the Karkheh River in Iran, and the rest is fed by branches of the Tigris River in Iraq.

Waste management is also one of the most critical challenges in the oil and gas drilling industry. Waste management includes two parts: wastewater management and rock cutting management. The main fluid used in drilling oil and gas wells in Iran is saturated polymer mud. The waste was dumped daily for various reasons and was carried to the corral pit. The water is separated from the dumped water-based mud. Daily water was directed to wash the drilling rig equipment and accumulated in the waste pit. The accumulation of this water is called wastewater. The current problem with wastewater in Iranian oil fields is its high chloride content that is discharged into the marsh. This is a serious problem that contaminates marsh water and threatens adjacent plant and animal life (Figure 8B). Although there are some methods, such as thermal approaches, to reduce the amount of chloride in wastewater, they are not cost-effective for drilling companies. Therefore, to prevent this problem, it is urgent to find a more operational, practical, and cost-effective way to reduce the amount of chloride in the large volume of daily wastewater. In addition to wastewater, rock cuttings obtained from drilling operations are another problem in the marsh. A typical well in the subjected oil field has a depth of 3500 m. Therefore, a whole volume of 3000 m^3 of cuttings is transferred from the bottom hole to the ground surface. If the average density of the cuttings is assumed to be 2 tons/m^3, an approximate tonnage of 6000 tons of crushed rock is brought to the surface of the marsh at the end of each wellbore drilling operation and is placed in preplanned landfills. At least 250 wells have been drilled in the marsh. Therefore, a total volume and tonnage of 750,000 m^3 and 1,500,000 tons have been dumped in the area.

5. Conclusions

Large-scale exploitation of natural resources is often accompanied by serious footprints on the local ecosystems. Detection and prevention of such environmental impacts are of paramount importance in terms of both regional and global perspectives on sustainable management. In this research, the most crucial impacts pertinent to the hydrocarbon exploitation in the Khuzestan province, Iran were studied and discussed. Since the province lies in the north of the Persian Gulf, the study area included both lands of the Khuzestan province along with the adjacent parts of the Persian Gulf.

The local seismic records together with the satellite data were utilized to detect, evaluate, and measure the severity of such different footprints in the area. Based on the results, it was deduced that the hydrocarbon production has vastly influenced the original lithosphere, hydrosphere, atmosphere, and biosphere.

Regarding the lithosphere, the hydrocarbon exploitation from the subsurface formations has remarkably disturbed the regional in situ stress state. This has led to frequent earthquakes originating from shallow depths of less than 15 km. Obviously, such shallow quakes may result in secondary problems such as groundwater table change, infrastructure instability, local ground movements, etc. Furthermore, it has also generated a noticeable land subsidence rate equal to 10–15 cm per year in the southern regions of the province. Since such regions are relatively flat, the seawater from the Persian Gulf flows through

those lands, thereby threatening the residual districts already established in the vicinity of the gulf.

Concerning the hydrosphere, it was found that in the northern and western regions of the Persian Gulf, the oil spill contamination spreads over the seawater surface during all days of the year. The presence of such long-term and resistant pollutants severely endangers the life of the native creatures and plants. In addition, another impact on the hydrosphere is the water drainage operations for drying the local marshes and preparing them for the preplanned drilling operations. This causes substantial dust propagation problems, transferring harmful and toxic particles throughout the entire atmosphere of the area. Consequently, the regional biosphere and the lives of native inhabitants, animals, and plants are deeply threatened.

To sum up, it is concluded that the harmful environmental impacts on the study area are very pressing issues that can even deteriorate the circumstances if urgent actions are not taken by regional and national authorities, companies, and policymakers. The results presented in this research can be used as an initial reference for addressing and reducing those environmental footprints.

Author Contributions: Conceptualization, Formal Analysis, Data Curation, Writing—Original Draft Preparation, Visualization, Methodology: H.R. and D.K. and M.A.M.Z.; Validation, Writing—Review and Editing, Supervision, Project Administration: D.K.; Software, Investigation, Resources: H.R. and M.A.M.Z. and D.K. All authors have read and agreed to the published version of the manuscript.

Funding: The project was supported by the AGH University of Science and Technology, Krakow, Poland, subsidy 16.16.190.779.

Data Availability Statement: The data are within the manuscript.

Acknowledgments: The authors acknowledge the support of AGH University of Science and Technology, Krakow, Poland. The authors also acknowledge the assistance from all staffs fromthe Institute of Geophysics, at the University of Tehran, Iran.

Conflicts of Interest: The authors declare no conflict of interest.

References

1. Ghorbani, M. *The Economic Geology of Iran: Mineral Deposits and Natural Resources*; Springer Geology: Dordrecht, The Netherlands, 2013; ISBN 978-94-007-5624-3.
2. Aung, T.S. Evaluation of the environmental impact assessment system and implementation in Myanmar: Its significance in oil and gas industry. *Environ. Impact Assess. Rev.* **2017**, *66*, 24–32. [CrossRef]
3. Khalilidermani, M.; Knez, D. A Survey of Application of Mechanical Specific Energy in Petroleum and Space Drilling. *Energies* **2022**, *15*, 3162. [CrossRef]
4. van der Voort, N.; Vanclay, F. Social impacts of earthquakes caused by gas extraction in the Province of Groningen, The Netherlands. *Environ. Impact Assess. Rev.* **2015**, *50*, 1–15. [CrossRef]
5. Herbut, A.; Khairutdinov, M.M.; Kongar-Syuryun, C.; Rybak, J. The surface wave attenuation as the effect of vibratory compaction of building embankments. *IOP Conf. Ser. Earth Environ. Sci.* **2019**, *362*, 012131. [CrossRef]
6. Khalilidermani, M.; Knez, D.; Zamani, M.A.M. Empirical Correlations between the Hydraulic Properties Obtained from the Geoelectrical Methods and Water Well Data of Arak Aquifer. *Energies* **2021**, *14*, 5415. [CrossRef]
7. Knez, D.; Rajaoalison, H.; Nkunzi, D. Drilling Mud Influence on Sandstone Poroelastic Parameters. *J. Geotechnol. Energy* **2022**, *39*, 5–13. [CrossRef]
8. Festa, G.; Picozzi, M.; Scala, A.; Zollo, A. Earthquake Seismology. In *Encyclopedia of Geology*, 2nd ed.; Alderton, D., Elias, S.A., Eds.; Academic Press: Cambridge, MA, USA, 2021; pp. 575–586, ISBN 978-0-08-102909-1.
9. Akoto, R.N.A.; Knez, D.; Atepor, L. VTI Anisotropy in Wellbore Strengthening Model. In Proceedings of the Sustainable Education and Development—Making Cities and Human Settlements Inclusive, Safe, Resilient, and Sustainable. Presented during Applied Research Conference in Africa 2021, Accra, Ghana, 25–28 August 2021; Mojekwu, J.N., Thwala, W., Aigbavboa, C., Bamfo-Agyei, E., Atepor, L., Oppong, R.A., Eds.; Springer International: Cham, Switzerland, 2022; pp. 245–256.
10. Green, J.P. An Approach to Analyzing Multiple Causes of Subsidence. Paper presented at the Fall Meeting of the Society of Petroleum Engineers of AIME, San Antonio, TX, USA, 8–11 October 1972. [CrossRef]
11. Hsü, K.J. Hazards—Causes and responses: 'Natural and anthropogenically induced hazards'. In Proceedings of the European Science Foundation Conference, Davos, Switzerland, 8–12 December 1991; Volume 2, pp. 345–348. [CrossRef]

12. Knez, D.; Rajaoalison, H. Discrepancy between measured dynamic poroelastic parameters and predicted values from Wyllie's equation for water-saturated Istebna sandstone. *Acta Geophys.* **2021**, *69*, 673–680. [CrossRef]
13. Knez, D.; Calicki, A. Looking for a new source of natural proppants in Poland. *Bull. Pol. Acad. Sci. Tech. Sci.* **2018**, *66*. [CrossRef]
14. Knez, D.; Khalilidermani, M. A Review of Different Aspects of Off-Earth Drilling. *Energies* **2021**, *14*, 7351. [CrossRef]
15. Knez, D.; Zamani, M.A.M. A Review of the Geomechanics Aspects in Space Exploration. *Energies* **2021**, *14*, 7522. [CrossRef]
16. Quosay, A.A.; Knez, D.; Ziaja, J. Hydraulic fracturing: New uncertainty based modeling approach for process design using Monte Carlo simulation technique. *PLoS ONE* **2020**, *15*, e0236726. [CrossRef] [PubMed]
17. Knez, D.; Zamani, M.A.M. Empirical Formula for Dynamic Biot Coefficient of Sandstone Samples from South-West of Poland. *Energies* **2021**, *14*, 5514. [CrossRef]
18. Rybak, J.; Khayrutdinov, M.M.; Kuziev, D.A.; Kongar-Syuryun, C.B.; Babyr, N.V. Prediction of the geomechanical state of the rock mass when mining salt deposits with stowing. *J. Min. Inst.* **2022**, *253*, 61–70. [CrossRef]
19. Chaussard, E.; Wdowinski, S.; Cabral-Cano, E.; Amelung, F. Land subsidence in central Mexico detected by ALOS InSAR time-series. *Remote Sens. Environ.* **2014**, *140*, 94–106. [CrossRef]
20. Corbau, C.; Simeoni, U.; Zoccarato, C.; Mantovani, G.; Teatini, P. Coupling land use evolution and subsidence in the Po Delta, Italy: Revising the past occurrence and prospecting the future management challenges. *Sci. Total Environ.* **2019**, *654*, 1196–1208. [CrossRef]
21. Galloway, D.L.; Burbey, T.J. Review: Regional land subsidence accompanying groundwater extraction. *Hydrogeol. J.* **2011**, *19*, 1459–1486. [CrossRef]
22. Du, Z.; Ge, L.; Ng, A.H.-M.; Zhu, Q.; Yang, X.; Li, L. Correlating the subsidence pattern and land use in Bandung, Indonesia with both Sentinel-1/2 and ALOS-2 satellite images. *Int. J. Appl. Earth Obs. Geoinf.* **2018**, *67*, 54–68. [CrossRef]
23. Knez, D.; Mazur, S. Simulation of Fracture Conductivity Changes Due to Proppant Composition and Stress Cycles. *Inż. Miner.* **2019**, *21*. [CrossRef]
24. Zhang, L. Big Data, Knowledge Mapping for Sustainable Development: A Water Quality Index Case Study. *Emerg. Sci. J.* **2019**, *3*, 249–254. [CrossRef]
25. Deng, F.; Dixon, T.H.; Xie, S. Surface Deformation and Induced Seismicity Due to Fluid Injection and Oil and Gas Extraction in Western Texas. *J. Geophys. Res. Solid Earth* **2020**, *125*, e2019JB018962. [CrossRef]
26. Knez, D.; Wiśniowski, R.; Owusu, W.A. Turning filling material into proppant for coalbed methane in Poland—Crush test results. *Energies* **2019**, *12*, 1820. [CrossRef]
27. Knez, D.; Rajaoalison, H. Land Subsidence Assessment for Wind Turbine Location in the South-Western Part of Madagascar. *Energies* **2022**, *15*, 4878. [CrossRef]
28. Pratt, W.E.; Johnson, D.W. Local Subsidence of the Goose Creek Oil Field. *J. Geol.* **1926**, *34*, 577–590. [CrossRef]
29. Rajaoalison, H.; Knez, D. Current trends in land subsidence of the North-Central part of Poland using DInSAR technique. *E3S Web Conf.* **2021**, *266*, 03006. [CrossRef]
30. Knez, D. Stress state analysis in aspect of wellbore drilling direction. *Arch. Min. Sci.* **2014**, *59*, 71–76. [CrossRef]
31. Rajaoalison, H.; Knez, D.; Zlotkowski, A. Changes of dynamic mechanical properties of brine-saturated Istebna sandstone under action of temperature and stress. *Przemysl Chem.* **2019**, *98*, 801–804. [CrossRef]
32. Zamani, M.A.M.; Knez, D. A New Mechanical-Hydrodynamic Safety Factor Index for Sand Production Prediction. *Energies* **2021**, *14*, 3130. [CrossRef]
33. Guzy, A.; Malinowska, A.A. Assessment of the Impact of the Spatial Extent of Land Subsidence and Aquifer System Drainage Induced by Underground Mining. *Sustainability* **2020**, *12*, 7871. [CrossRef]
34. Ng, A.H.-M.; Ge, L.; Li, X. Assessments of land subsidence in the Gippsland Basin of Australia using ALOS PALSAR data. *Remote Sens. Environ.* **2015**, *159*, 86–101. [CrossRef]
35. Pérez-Falls, Z.; Martínez-Flores, G.; Sarychikhina, O. Land Subsidence Detection in the Coastal Plain of Tabasco, Mexico Using Differential SAR Interferometry. *Land* **2022**, *11*, 1473. [CrossRef]
36. Liu, Y.; Huang, H.; Liu, Y.; Bi, H. Linking land subsidence over the Yellow River delta, China, to hydrocarbon exploitation using multi-temporal InSAR. *Nat. Hazards* **2016**, *84*, 271–291. [CrossRef]
37. Kuzmin, Y.O. Deformation Consequences of the Development of Oil and Gas Field. *Izv. Atmospheric Ocean. Phys.* **2021**, *57*, 1479–1497. [CrossRef]
38. Macini, P.; Mesini, E.; Panei, L.; Terlizzese, F. Land subsidence, seismicity and pore pressure monitoring: The new requirements for the future development of oil and gas fields in Italy. *Proc. Int. Assoc. Hydrol. Sci.* **2015**, *372*, 533–538. [CrossRef]
39. Bailey, R.H.; Engelhardt, F.R. Environmental management of offshore oil and gas activities in Canada. *Environ. Impact Assess. Rev.* **1983**, *4*, 523–538. [CrossRef]
40. Vora, M.; Sanni, S.; Flage, R. An environmental risk assessment framework for enhanced oil recovery solutions from offshore oil and gas industry. *Environ. Impact Assess. Rev.* **2021**, *88*, 106512. [CrossRef]
41. Wilhelmsson, D.; Thompson, R.C.; Holmström, K.; Lindén, O.; Eriksson-Hägg, H. Chapter 6—Marine Pollution. In *Managing Ocean Environments in a Changing Climate*; Noone, K.J., Sumaila, U.R., Diaz, R.J., Eds.; Elsevier: Boston, UK, 2013; pp. 127–169. ISBN 978-0-12-407668-6.
42. Fiscella, B.; Giancaspro, A.; Nirchio, F.; Pavese, P.; Trivero, P. Oil spill detection using marine SAR images. *Int. J. Remote Sens.* **2010**, *21*, 3561–3566. [CrossRef]

43. Lu, J. Marine oil spill detection, statistics and mapping with ERS SAR imagery in south-east Asia. *Int. J. Remote Sens.* **2010**, *24*, 3013–3032. [CrossRef]
44. Pisano, A.; De Dominicis, M.; Biamino, W.; Bignami, F.; Gherardi, S.; Colao, F.; Coppini, G.; Marullo, S.; Sprovieri, M.; Trivero, P.; et al. An oceanographic survey for oil spill monitoring and model forecasting validation using remote sensing and in situ data in the Mediterranean Sea. *Deep. Sea Res. Part II Top. Stud. Oceanogr.* **2016**, *133*, 132–145. [CrossRef]
45. Marghany, M.; Hashim, M. Comparison between Mahalanobis classification and neural network for oil spill detection using RADARSAT-1 SAR data. *Int. J. Phys. Sci.* **2011**, *6*, 566–576. [CrossRef]
46. Shu, Y.; Li, J.; Yousif, H.; Gomes, G. Dark-spot detection from SAR intensity imagery with spatial density thresholding for oil-spill monitoring. *Remote Sens. Environ.* **2010**, *114*, 2026–2035. [CrossRef]
47. Naz, S.; Iqbal, M.F.; Mahmood, I.; Allam, M. Marine oil spill detection using Synthetic Aperture Radar over Indian Ocean. *Mar. Pollut. Bull.* **2021**, *162*, 111921. [CrossRef] [PubMed]
48. de la Huz, R.; Lastra, M.; López, J. Oil Spills. In *Encyclopedia of Environmental Health*; Nriagu, J.O., Ed.; Elsevier: Burlington, NJ, USA, 2011; pp. 251–255. ISBN 978-0-444-52272-6.
49. Rodríguez, J.G.; Incera, M.; de la Huz, R.; López, J.; Lastra, M. Polycyclic aromatic hydrocarbons (PAHs), organic matter quality and meiofauna in Galician sandy beaches, 6 months after the Prestige oil-spill. *Mar. Pollut. Bull.* **2007**, *54*, 1046–1052. [CrossRef] [PubMed]
50. Rybak, J.; Gorbatyuk, S.M.; Bujanovna-Syuryun, K.C.; Khairutdinov, A.M.; Tyulyaeva, Y.S.; Makarov, P.S. Utilization of Mineral Waste: A Method for Expanding the Mineral Resource Base of a Mining and Smelting Company. *Metallurgist* **2021**, *64*, 851–861. [CrossRef]
51. Tcvetkov, P.; Cherepovitsyn, A.; Fedoseev, S. Public perception of carbon capture and storage: A state-of-the-art overview. *Heliyon* **2019**, *5*, e02845. [CrossRef] [PubMed]
52. Berberian, M. The southern Caspian: A compressional depression floored by a trapped, modified oceanic crust. *Can. J. Earth Sci.* **1983**, *20*, 163–183. [CrossRef]
53. Berberian, M.; King, G.C.P. Towards a paleogeography and tectonic evolution of Iran. *Can. J. Earth Sci.* **1981**, *18*, 210–265. [CrossRef]
54. Stampfli, G.M.; Borel, G.D. A plate tectonic model for the Paleozoic and Mesozoic constrained by dynamic plate boundaries and restored synthetic oceanic isochrons. *Earth Planet. Sci. Lett.* **2002**, *196*, 17–33. [CrossRef]
55. Teknik, V.; Thybo, H.; Artemieva, I.M.; Ghods, A. A new tectonic map of the Iranian plateau based on aeromagnetic identification of magmatic arcs and ophiolite belts. *Tectonophysics* **2020**, *792*, 228588. [CrossRef]
56. Beydoun, Z.R. *The Middle East: Regional Geology and Petroleum Reserves*; Scientific Surveys Ltd.: Beaconsfield, UK, 1988; ISBN 978-0-901360-21-2.
57. Alsharhan, A.S.; Nairn, A.E.M. *Sedimentary Basins and Petroleum Geology of the Middle East*; Elsevier Science: Amsterdam, The Netherlands, 1997; ISBN 978-0-444-82465-3.
58. Al-Husseini, M. The debate over Hubbert's Peak: A review. *GeoArabia* **2006**, *11*, 181–210. [CrossRef]
59. Rezapour, M. Magnitude Scale in the Tabriz Seismic Network. *J. Earth Space Phys.* **2005**, *31*, 13–21.
60. Taghizadeh-Farahmand, F.; Afsari, N.; Sodoudi, F. Crustal Thickness of Iran Inferred from Converted Waves. *Pure Appl. Geophys.* **2015**, *172*, 309–331. [CrossRef]
61. Javadi, S.; Taghizadeh-Farahmand, F.; Gheitanchi, M.R. Seismic images of crust and upper mantle in Central Iran (from Jiroft to Ashtian) via teleseismic waves. *Contrib. Geophys. Geod.* **2020**, *50*, 395–412. [CrossRef]
62. Moradi, A.S.; Hatzfeld, D.; Tatar, M. Microseismicity and seismotectonics of the North Tabriz fault (Iran). *Tectonophysics* **2011**, *506*, 22–30. [CrossRef]
63. Nuttli, O.W. Seismic wave attenuation and magnitude relations for eastern North America. *J. Geophys. Res.* **1973**, *78*, 876–885. [CrossRef]
64. Tanner, D.C.; Buness, H.; Igel, J.; Günther, T.; Gabriel, G.; Skiba, P.; Plenefisch, T.; Gestermann, N.; Walter, T.R. Chapter 3—Fault detection. In *Understanding Faults*; Tanner, D., Brandes, C., Eds.; Elsevier: Amsterdam, The Netherlands, 2020; pp. 81–146, ISBN 978-0-12-815985-9.
65. Ekström, G. 4.18—Global Seismicity: Results from Systematic Waveform Analyses, 1976–2012. In *Treatise on Geophysics*, 2nd ed.; Schubert, G., Ed.; Elsevier: Oxford, UK, 2015; pp. 467–475. ISBN 978-0-444-53803-1.
66. Hosseini, H.; Pakzad, M.; Naserieh, S. Iranian regional centroid moment tensor catalog: Solutions for 2012–2017. *Phys. Earth Planet. Inter.* **2019**, *286*, 29–41. [CrossRef]
67. Dziewonski, A.M.; Chou, T.-A.; Woodhouse, J.H. Determination of earthquake source parameters from waveform data for studies of global and regional seismicity. *J. Geophys. Res. Solid Earth* **1981**, *86*, 2825–2852. [CrossRef]
68. Wessel, P.; Luis, J.F.; Uieda, L.; Scharroo, R.; Wobbe, F.; Smith, W.H.F.; Tian, D. The Generic Mapping Tools Version 6. *Geochem. Geophys. Geosystems* **2019**, *20*, 5556–5564. [CrossRef]
69. Rahmati, O.; Golkarian, A.; Biggs, T.; Keesstra, S.; Mohammadi, F.; Daliakopoulos, I.N. Land subsidence hazard modeling: Machine learning to identify predictors and the role of human activities. *J. Environ. Manag.* **2019**, *236*, 466–480. [CrossRef]
70. Guoqing, Y.; Jingqin, M. D-InSAR Technique for Land Subsidence Monitoring. *Earth Sci. Front.* **2008**, *15*, 239–243. [CrossRef]
71. Herrera, G.; Tomás, R.; López-Sánchez, J.M.; Delgado, J.; Mallorqui, J.J.; Duque, S.; Mulas, J. Advanced DInSAR analysis on mining areas: La Union case study (Murcia, SE Spain). *Eng. Geol.* **2007**, *90*, 148–159. [CrossRef]

72. Wang, Z.; Zhang, J.; Huang, G.; Zhang, Y. Monitoring Land Subsidence in Suzhou City Using D-InSAR Technique. In Proceedings of the 2009 2nd International Congress on Image and Signal Processing, Tianjin, China, 17–19 October 2009; pp. 1–4.
73. Serco Italia SPA Land Subsidence with Sentinel-1 Using SNAP. (Version 1.2), 2018. Retrieved from RUS Lectures. Available online: https://rus-copernicus.eu/portal/the-rus-library/learn-by-yourself/ (accessed on 15 August 2022).
74. Zebker, H.A.; Rosen, P.A.; Hensley, S. Atmospheric effects in interferometric synthetic aperture radar surface deformation and topographic maps. *J. Geophys. Res. Solid Earth* **1997**, *102*, 7547–7563. [CrossRef]
75. Hanssen, R.F. *Radar Interferometry: Data Interpretation and Error Analysis*; Remote Sensing and Digital Image Processing; Springer: Dordrecht, The Netherlands, 2001; ISBN 978-0-7923-6945-5.
76. Massonnet, D.; Rossi, M.; Carmona, C.; Adragna, F.; Peltzer, G.; Feigl, K.; Rabaute, T. The displacement field of the Landers earthquake mapped by radar interferometry. *Nature* **1993**, *364*, 138–142. [CrossRef]
77. Fingas, M.; Brown, C.E. A Review of Oil Spill Remote Sensing. *Sensors* **2018**, *18*, 91. [CrossRef] [PubMed]
78. Zhao, J.; Temimi, M.; Azhar, M.A.; Ghedira, H. Satellite-Based Tracking of Oil Pollution in the Arabian Gulf and the Sea of Oman. *Can. J. Remote Sens.* **2015**, *41*, 113–125. [CrossRef]
79. Brekke, C.; Solberg, A.H.S. Oil spill detection by satellite remote sensing. *Remote Sens. Environ.* **2005**, *95*, 1–13. [CrossRef]
80. Fingas, M.; Brown, C. Review of oil spill remote sensing. *Mar. Pollut. Bull.* **2014**, *83*, 9–23. [CrossRef]
81. Ajadi, O.A.; Meyer, F.J.; Tello, M.; Ruello, G. Oil Spill Detection in Synthetic Aperture Radar Images Using Lipschitz-Regularity and Multiscale Techniques. *IEEE J. Sel. Top. Appl. Earth Obs. Remote Sens.* **2018**, *11*, 2389–2405. [CrossRef]
82. Fan, H.D.; Cheng, D.; Deng, K.Z.; Chen, B.Q.; Zhu, C.G. Subsidence monitoring using D-InSAR and probability integral prediction modelling in deep mining areas. *Surv. Rev.* **2015**, *47*, 438–445. [CrossRef]
83. Topouzelis, K.; Singha, S. Chapter 6—Oil Spill Detection Using Space-Borne Sentinel-1 SAR Imagery. In *Oil Spill Science and Technology*, 2nd ed.; Fingas, M., Ed.; Gulf Professional Publishing: Boston, UK, 2017; pp. 387–402. ISBN 978-0-12-809413-6.
84. Alpers, W.; Holt, B.; Zeng, K. Oil spill detection by imaging radars: Challenges and pitfalls. *Remote Sens. Environ.* **2017**, *201*, 133–147. [CrossRef]
85. Migliaccio, M.; Nunziata, F.; Buono, A. SAR polarimetry for sea oil slick observation. *Int. J. Remote Sens.* **2015**, *36*, 3243–3273. [CrossRef]
86. Skrunes, S.; Brekke, C.; Eltoft, T. Oil spill characterization with multi-polarization C- and X-band SAR. In Proceedings of the 2012 IEEE International Geoscience and Remote Sensing Symposium, Munich, Germany, 22–27 July 2012; pp. 5117–5120.
87. Wisen, J.; Chesnaux, R.; Wendling, G.; Werring, J.; Barbecot, F.; Baudron, P. Assessing the potential of cross-contamination from oil and gas hydraulic fracturing: A case study in northeastern British Columbia, Canada. *J. Environ. Manag.* **2019**, *246*, 275–282. [CrossRef] [PubMed]
88. Luisa Martínez, M.; Mendoza-González, G.; Silva-Casarín, R.; Mendoza-Baldwin, E. Land use changes and sea level rise may induce a "coastal squeeze" on the coasts of Veracruz, Mexico. *Glob. Environ. Change* **2014**, *29*, 180–188. [CrossRef]
89. Feitelson, E.; Tubi, A. A main driver or an intermediate variable? Climate change, water and security in the Middle East. *Glob. Environ. Change* **2017**, *44*, 39–48. [CrossRef]
90. Sheppard, C.R.C. Physical environment of the Gulf relevant to marine pollution: An overview. *Mar. Pollut. Bull.* **1993**, *27*, 3–8. [CrossRef]
91. Kamranzad, B. Persian Gulf zone classification based on the wind and wave climate variability. *Ocean Eng.* **2018**, *169*, 604–635. [CrossRef]
92. de la Huz, R.; Lastra, M.; Junoy, J.; Castellanos, C.; Viéitez, J.M. Biological impacts of oil pollution and cleaning in the intertidal zone of exposed sandy beaches: Preliminary study of the "Prestige" oil spill. *Estuar. Coast. Shelf Sci.* **2005**, *65*, 19–29. [CrossRef]
93. Feder, H.M.; Blanchard, A. The deep benthos of Prince William Sound, Alaska, 16 months after the Exxon Valdez oil spill. *Mar. Pollut. Bull.* **1998**, *36*, 118–130. [CrossRef]
94. Hayes, M.O.; Michel, J. Factors determining the long-term persistence of Exxon Valdez oil in gravel beaches. *Mar. Pollut. Bull.* **1999**, *38*, 92–101. [CrossRef]
95. Peterson, C.H. The "Exxon Valdez" oil spill in Alaska: Acute, indirect and chronic effects on the ecosystem. In *Advances in Marine Biology*; Academic Press: Cambridge, MA, USA, 2001; Volume 39, pp. 1–103.
96. Dhaka, A.; Chattopadhyay, P. A review on physical remediation techniques for treatment of marine oil spills. *J. Environ. Manag.* **2021**, *288*, 112428. [CrossRef]
97. Liu, X. Integrated modeling of oil spill response strategies: A coastal management case study. *Environ. Sci. Policy* **2010**, *13*, 415–422. [CrossRef]
98. Abdullah, K.; Stenstrom, M.; Suffet, I.M.; Swamikannu, X.; Malloy, T. Regulating oil and gas facility stormwater discharge: An assessment of surface impoundments, spills, and permit compliance. *Environ. Sci. Policy* **2017**, *76*, 139–145. [CrossRef]
99. Ornitz, B.E.; Champ, M.A. *Oil Spills First Principles: Prevention and Best Response*, 1st ed.; Elsevier: Amsterdam, NY, USA, 2002; ISBN 978-0-08-042814-7.
100. Whitfield, J. How to clean a beach. *Nature* **2003**, *422*, 464–466. [CrossRef] [PubMed]
101. Zengel, S.A.; Michel, J. Vegetation cutting as a clean-up method for salt and brackish marshes impacted by oil spills: A review and case history of the effects on plant recovery. *Mar. Pollut. Bull.* **1996**, *32*, 876–885. [CrossRef]
102. Alobaidi, L.; Iraq, N.; Dijlah, H. Iraq and Iran's Hawizeh Marshes: Threats and Opportunities. Save Tigris 2018. Available online: https://osme.org/2018/04/iraq-and-irans-hawizeh-marshes-threats-and-opportunities/ (accessed on 24 October 2022).